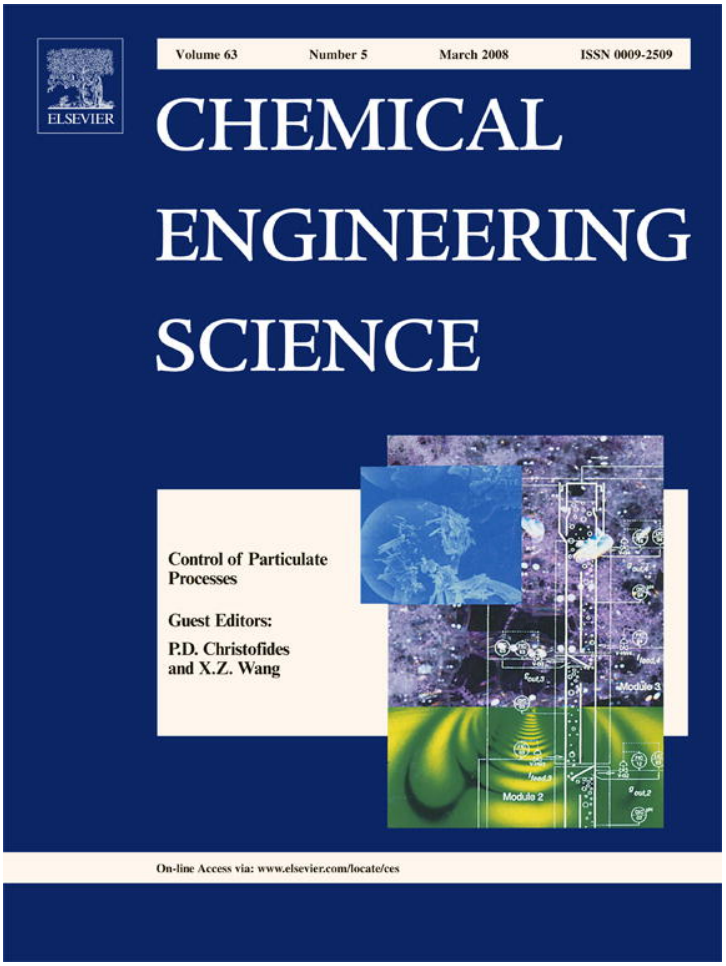

ELSEVIER

Chemical Engineering Science 63 (2008) 1217–1229

Chemical Engineering Science

www.elsevier.com/locate/ces

Handling sensor malfunctions in control of particulate processes

Adiwinata Gani[a], Prashant Mhaskar[b], Panagiotis D. Christofides[a,*]

[a]*Department of Chemical and Biomolecular Engineering, University of California, Los Angeles, CA 90095, USA*
[b]*Department of Chemical Engineering, McMaster University, Hamilton, Ont., Canada L8S 4L7*

Available online 22 July 2007

Abstract

This work focuses on feedback control of particulate processes in the presence of sensor data losses. Two typical particulate process examples, a continuous crystallizer and a batch protein crystallizer, modeled by population balance models (PBMs), are considered. In the case of the continuous crystallizer, a Lyapunov-based nonlinear output feedback controller is first designed on the basis of an approximate moment model and is shown to stabilize an open-loop unstable steady-state of the PBM in the presence of input constraints. Then, the problem of modeling sensor data losses is investigated and the robustness of the nonlinear controller with respect to data losses is extensively investigated through simulations. In the case of the batch crystallizer, a predictive controller is first designed to obtain a desired crystal size distribution at the end of the batch while satisfying state and input constraints. Subsequently, we point out how the constraints in the predictive controller can be modified as a means of achieving constraint satisfaction in the closed-loop system in the presence of sensor data losses.

Keywords: Population balance model; Model reduction; Lyapunov-based control; Predictive control; Input constraints; Sensor malfunctions; Crystallization processes

1. Introduction

Particulate processes play a key role in a broad range of process industries ranging from chemical, materials and minerals to agricultural, food and pharmaceutical. These areas of manufacturing have a current value exceeding, according to some estimates, two trillion dollars and a growth factor of 5 to 10 over the next decade. Examples include the crystallization of proteins for pharmaceutical applications, the emulsion polymerization for the production of latex, the fluidized bed production of solar-grade silicon particles through thermal decomposition of silane gas and the aerosol synthesis of titania powder used in the production of white pigments. Particulate processes are widely recognized as presenting a number of processing challenges which are not encountered in gas or liquid processes. One of these challenges is to operate the particulate process in a way that it consistently makes products with a desired particle size distribution (PSD). For example, in crystallization processes, the shape of the crystal size distribution is an important quality index which strongly affects crystal function and downstream processing such as filtration, centrifugation and milling (Rawlings et al., 1993).

Population balances have provided a natural framework for the mathematical modeling of PSDs (see, for example, the tutorial article (Hulburt and Katz, 1964) and the review article (Ramkrishna, 1985)), and have been successfully used to describe PSDs in many particulate processes. Population balance modeling of particulate processes typically leads to systems of nonlinear partial integro-differential equations that describe the rate of change of the PSD. The population balance models (PBMs) are also coupled with the material, momentum and energy balances that describe the rate of change of the state variables of the continuous phase, leading to complete particulate process models. In the context of PBM-based control of particulate processes, the main difficulty in synthesizing practically implementable nonlinear feedback controllers is the distributed parameter nature of the PBMs which does not allow their direct use for the synthesis of low-order (and therefore, practically implementable) nonlinear output feedback controllers. To overcome this problem, we took advantage of the property that the dominant dynamic behavior of many particulate process models

* Corresponding author. Tel.: +1 3107941015; fax: +1 3102064107.
E-mail address: pdc@seas.ucla.edu (P.D. Christofides).

0009-2509/$ - see front matter © 2007 Elsevier Ltd. All rights reserved.
doi:10.1016/j.ces.2007.07.020

is low-dimensional and proposed (Chiu and Christofides, 1999) a model reduction procedure, based on a combination of the method of weighted residuals and the concept of approximate inertial manifold, which leads to the construction of low-order ordinary differential equation (ODE) systems that accurately reproduce the dominant dynamics of broad classes of particulate process models. These ODE systems were subsequently used for the synthesis of nonlinear (Chiu and Christofides, 1999; Kalani and Christofides, 1999; Christofides, 2002), robust (Chiu and Christofides, 2000; El-Farra et al., 2001), and predictive (Shi et al., 2005, 2006) controllers that enforce desired stability, performance, robustness and constraint handling properties in the closed-loop system. Owing to the low-dimensional structure of the controllers, the computation of the control action involves the solution of a small set of ODEs, and thus, the developed controllers can be readily implemented in real-time with reasonable computing power. In addition to these results, an online optimal control methodology including various performance objectives was developed for a seeded batch cooling crystallizer in Xie et al. (2001) and Zhang and Rohani (2003). The reader may refer to Daoutidis and Henson (2002), Doyle et al. (2002), Braatz and Hasebe (2002) and Christofides et al. (2007) for reviews of results on simulation and control of particulate processes.

Despite this progress on the design of advanced feedback control systems for particulate processes, the problem of investigating controller stability, performance and robustness in the presence of sensor data losses has received no attention. Sensor data losses may arise due to a host of reasons including measurement sample loss, intermittent failures associated with measurement techniques, as well as those induced via data packet losses over transmission lines. Previous work on control subject to actuator/sensor faults has exclusively focused on lumped parameter systems. Specifically, in El-Farra et al. (2005), communication losses were modeled as delays in implementing the control action and in Mhaskar et al. (2006) the problem of unavailability of some of the states for measurement was considered and reconfiguration-based strategies were devised to achieve fault-tolerance subject to faults in the control actuators. Furthermore, in Mhaskar et al. (2007), a theoretical framework was developed for the modeling, analysis and reconfiguration-based fault-tolerant control of nonlinear processes subject to asynchronous sensor data losses (intermittent unavailability of measurements). Specifically, for each control configuration, the stability region (i.e., the set of initial conditions starting from where closed-loop stabilization under continuous availability of measurements is guaranteed) as well as the maximum allowable data loss rate which preserves closed-loop stability was computed and this characterization was utilized in taking preventive action, i.e., to trigger reconfiguration, as well as in making the decision as to which backup configuration should be employed in the closed-loop system to maintain stability. The method was applied to a lumped polyethylene reactor model.

This work focuses on the problem of feedback control of particulate processes in the presence of sensor data losses. Two typical particulate process examples, a continuous crystallizer and a batch protein crystallizer, are considered and are modeled by PBMs. In the case of the continuous crystallizer, a Lyapunov-based nonlinear output feedback controller is first designed on the basis of an approximate moment model and is shown to stabilize an open-loop unstable steady-state of the PBM in the presence of input constraints. Then, the robustness of the nonlinear controller with respect to data losses is extensively investigated through simulations. In the case of the batch crystallizer, a predictive controller is first designed to obtain a crystal size distribution at the end of the batch that has desired shape while satisfying state and input constraints. Subsequently, we point out how the constraints in the predictive controller can be modified as a means of achieving constraint satisfaction in the closed-loop system in the presence of sensor data losses. Extensive simulations are presented to demonstrate the effect of sensor data losses on closed-loop stability and performance in both examples.

2. Handling sensor malfunctions: continuous crystallizer

In the present section, we consider a standard model of a continuous crystallizer and address the problem of stabilization of its open-loop unstable steady-state using both state feedback and output feedback control in the presence of sensor data losses. We begin with the presentation of the crystallizer model, continue with the controller design and modeling of sensor data losses and conclude with extensive simulation results and discussion.

2.1. PBM of a continuous crystallizer

We consider a continuous crystallizer which is fed by a stream of solute at concentration c_0. Under the assumptions of isothermal operation, constant volume, mixed suspension, nucleation of crystals of infinitesimal size and mixed product removal, a dynamic model for a continuous crystallizer can be derived from a population balance for the particle phase and a mass balance for the solute concentration of the following form (Lei et al., 1971; Jerauld et al., 1983):

$$\frac{\partial n}{\partial \bar{t}} = -\frac{\partial (R(\bar{t})n)}{\partial r} - \frac{n}{\tau} + \delta(r-0)Q(\bar{t}),$$
$$\frac{\mathrm{d}c}{\mathrm{d}\bar{t}} = \frac{(c_0-\rho)}{\bar{\varepsilon}\tau} + \frac{(\rho-c)}{\tau} + \frac{(\rho-c)}{\bar{\varepsilon}}\frac{\mathrm{d}\bar{\varepsilon}}{\mathrm{d}\bar{t}}, \quad (1)$$

where $n(r,\bar{t})$ is the density of crystals of radius $r \in [0,\infty)$ at time $\bar{t}$ in the suspension, τ is the residence time, c is the solute concentration in the crystallizer, c_0 is the solute concentration in the feed and $\bar{\varepsilon}=1-\int_0^\infty n(r,\bar{t})\frac{4}{3}\pi r^3\,\mathrm{d}r$ is the volume of liquid per unit volume of suspension. $R(\bar{t})$ is the growth rate, $\delta(r-0)$ is the standard Dirac function, and $Q(\bar{t})$ is the nucleation rate. The term $\delta(r-0)Q(\bar{t})$ accounts for the production of crystals of infinitesimal (zero) size via nucleation. $R(\bar{t})$ and $Q(\bar{t})$ are assumed to follow McCabe's law and Volmer's nucleation law,

Table 1
Process parameters of the continuous crystallizer

$c_0 = 1000.0\,\mathrm{kg/m^3}$
$c_s = 980.2\,\mathrm{kg/m^3}$
$c_{0s} = 999.943\,\mathrm{kg/m^3}$
$\rho = 1770.0\,\mathrm{kg/m^3}$
$\tau = 1.0\,\mathrm{h}$
$k_1 = 5.065 \times 10^{-2}\,\mathrm{mm\,m^3\,kg^{-1}\,h^{-1}}$
$k_2 = 7.958\,\mathrm{mm^{-3}\,h^{-1}}$
$k_3 = 1.217 \times 10^{-3}$

respectively:

$$R(\bar{t}) = k_1(c - c_s),$$
$$Q(\bar{t}) = \bar{\varepsilon} k_2 \exp\left[-\frac{k_3}{(c/c_s - 1)^2}\right], \tag{2}$$

where k_1, k_2 and k_3 are constants and c_s is the concentration of solute at saturation.

A spatial discretization scheme based on Galerkin's method with 1000 spatial modes was used to obtain the solution of the system of Eqs. (1)–(2) (simulations of the system using more discretization modes led to identical results). The values of the process parameters used in the simulations can be found in Table 1. The crystallizer exhibits highly oscillatory behavior, which is the result of the interplay between growth and nucleation caused by the relative nonlinearity of the nucleation rate as compared to the growth rate (compare the nonlinear dependence of $Q(\bar{t})$ and $R(\bar{t})$ on c in Eq. (2)). To establish that the dynamics of the crystallizer are characterized by a small number of degrees of freedom, the method of moments is applied to the system of Eqs. (1)–(2) to derive an approximate ODE model. Specifically, the jth moment of $n(r, \bar{t})$ is defined as

$$\mu_j = \int_0^\infty r^j n(r, \bar{t})\,\mathrm{d}r, \quad j = 0, \ldots, \tag{3}$$

and upon multiplying the population balance in Eq. (1) by r^j, integrating over all particle sizes, and introducing the following set of dimensionless variables and parameters:

$$\tilde{x}_0 = 8\pi\sigma^3\mu_0, \quad \tilde{x}_1 = 8\pi\sigma^2\mu_1, \quad \tilde{x}_2 = 4\pi\sigma\mu_2,$$
$$\tilde{x}_3 = \tfrac{4}{3}\pi\mu_3, \ldots,$$
$$t = \frac{\bar{t}}{\tau}, \quad \sigma = k_1\tau(c_{0s} - c_s), \quad Da = 8\pi\sigma^3 k_2\tau,$$
$$F = \frac{k_3 c_s^2}{(c_{0s} - c_s)^2}, \quad \alpha = \frac{(\rho - c_s)}{(c_{0s} - c_s)},$$
$$\tilde{y} = \frac{(c - c_s)}{(c_{0s} - c_s)}, \quad u = \frac{(c_0 - c_{0s})}{(c_{0s} - c_s)}, \tag{4}$$

where c_{0s} is the steady-state solute concentration in the feed, the dominant dynamics of the process of Eq. (1) can be adequately captured by the fifth-order moments model which includes the dynamics of the first four moments and those of the solute concentration in the following form:

$$\frac{\mathrm{d}\tilde{x}_0}{\mathrm{d}t} = -\tilde{x}_0 + (1 - \tilde{x}_3) Da\, \mathrm{e}^{-F/\tilde{y}^2},$$
$$\frac{\mathrm{d}\tilde{x}_1}{\mathrm{d}t} = -\tilde{x}_1 + \tilde{y}\tilde{x}_0,$$
$$\frac{\mathrm{d}\tilde{x}_2}{\mathrm{d}t} = -\tilde{x}_2 + \tilde{y}\tilde{x}_1,$$
$$\frac{\mathrm{d}\tilde{x}_3}{\mathrm{d}t} = -\tilde{x}_3 + \tilde{y}\tilde{x}_2,$$
$$\frac{\mathrm{d}\tilde{y}}{\mathrm{d}t} = \frac{1 - \tilde{y} - (\alpha - \tilde{y})\tilde{y}\tilde{x}_2}{1 - \tilde{x}_3} + \frac{u}{1 - \tilde{x}_3}, \tag{5}$$

where $\tilde{x}_v$, $v = 0, 1, 2, 3$, are dimensionless moments of the crystal size distribution, $\tilde{y}$ is dimensionless concentration of the solute in the crystallizer and u is a dimensionless concentration of the solute in the feed. Note that the moments of order 4 and higher do not affect those of order 3 and lower, and moreover, the state of the infinite dimensional system is bounded when $\tilde{x}_3$ and $\tilde{y}$ are bounded, and it converges to a globally exponentially stable equilibrium point when $\lim_{t\to\infty} \tilde{x}_3 = c_1$ and $\lim_{t\to\infty} \tilde{y} = c_2$, where c_1, c_2 are constants. The reader may refer to El-Farra et al. (2001) for a detailed derivation of the moments model, and to Christofides (2002) for further results and references in this area. The stability properties of the fifth-order model of Eq. (5) have been also studied and it has been shown Jerauld et al. (1983) that the global phase space of this model has a unique unstable steady-state surrounded by a stable periodic orbit, and that the linearization of the system of Eq. (1) around the unstable steady-state includes two isolated complex conjugate eigenvalues with a positive real part.

2.2. Bounded Lyapunov-based control

Having obtained a low-order ODE model that captures the dominant dynamics of the continuous crystallizer, we proceed in this section to address the controller synthesis problem on the basis of the low-order model of Eq. (5). The control objective is to stabilize the crystallizer at an unstable steady-state (which corresponds to a desired PSD) using constrained control action. To this end, we initially rewrite the moments model of Eq. (5) in a more compact form:

$$\dot{\tilde{x}}(t) = f(\tilde{x}(t)) + g(\tilde{x}(t))\tilde{u}(t),$$
$$|u| \leqslant u_{\max},$$
$$\tilde{z}(t) = h(\tilde{x}(t)), \tag{6}$$

where $\tilde{x} = [\tilde{x}_0\ \tilde{x}_1\ \tilde{x}_2\ \tilde{x}_3\ \tilde{y}]'$, $\tilde{x}_v = x_v - x_v^s$, $v = 0, 1, 2, 3$, $\tilde{z} = z - z^s$, $\tilde{u} = u - u^s$, $u_{\max} > 0$ denotes the bound on the manipulated input, the superscript at x_v^s refers to the unstable steady-state at which we would like to asymptotically stabilize the system, $h(\tilde{x}(t)) = \tilde{x}_0$ and z denotes the measured output. In the system

of Eq. (6), f and g have the following form:

$$f(\tilde{x}) = \begin{bmatrix} -\tilde{x}_0 + (1-\tilde{x}_3)Da\, e^{-F/\tilde{y}^2} \\ -\tilde{x}_1 + \tilde{y}\tilde{x}_0 \\ -\tilde{x}_2 + \tilde{y}\tilde{x}_1 \\ -\tilde{x}_3 + \tilde{y}\tilde{x}_2 \\ \dfrac{1-\tilde{y}-(\alpha-\tilde{y})\tilde{y}\tilde{x}_2}{1-\tilde{x}_3} \end{bmatrix},$$

$$g(\tilde{x}) = \begin{bmatrix} 0 \\ 0 \\ 0 \\ 0 \\ 1 \\ \dfrac{1}{1-\tilde{x}_3} \end{bmatrix}.$$

Next we will review the design procedure of the bounded controller through state feedback and output feedback approaches. In the state feedback problem, measurements of $\tilde{x}_v(t)$ and $\tilde{y}(t)$ are assumed to be available for all t. In the output feedback problem, with the measurements of only $\tilde{z} = \tilde{x}_0$ available, the controller is constructed through a standard combination of a state feedback controller with a state observer. The state feedback controller is synthesized via Lyapunov techniques and the state observer is an extended Luenberger-type observer.

2.2.1. State feedback control

Consider the system of Eq. (6), for which a control Lyapunov function (CLF), $V(\tilde{x})$, is available. Using the CLF, we construct, using the results in Lin and Sontag (1991) (see also El-Farra and Christofides, 2001, 2003), the following continuous bounded control law:

$$u(\tilde{x}) = -k(\tilde{x})L_g V(\tilde{x}), \tag{7}$$

where

$$k(\tilde{x}) = \begin{cases} \dfrac{L_f V(\tilde{x}) + \sqrt{(L_f V(\tilde{x}))^2 + (u_{\max} L_g V(\tilde{x}))^4}}{(L_g V(\tilde{x}))^2[1 + \sqrt{1 + (u_{\max} L_g V(\tilde{x}))^2}]}, & L_g V(\tilde{x}) \neq 0, \\ 0, & L_g V(\tilde{x}) = 0, \end{cases} \tag{8}$$

where $L_f V(\tilde{x}) = (\partial V(\tilde{x})/\partial \tilde{x}) f(\tilde{x})$, and $L_g V(\tilde{x}) = (\partial V(\tilde{x})/\partial \tilde{x})$ $g(\tilde{x})$. An estimate of the constrained stability region of the above controller can be obtained using the level sets of V, i.e.,

$$\Omega = \{\tilde{x} \in \mathbb{R}^n : V(\tilde{x}) \leqslant c^{\max}\}, \tag{9}$$

where $c^{\max} > 0$ is the largest number for which every nonzero element of Ω is fully contained in the set:

$$\Phi = \{\tilde{x} \in \mathbb{R}^n : L_f V(\tilde{x}) < u_{\max} |L_g V(\tilde{x})|\}. \tag{10}$$

2.2.2. Output feedback control

Under the hypothesis that the system of Eq. (6) is locally observable (that is, its linearization around the desired operating steady-state is observable), the practical implementation of a nonlinear state feedback controller of the form of Eq. (7) will be achieved by employing the following nonlinear state observer:

$$\frac{d\omega}{dt} = f(\omega) + g(\omega)u + L(\tilde{z} - h(\omega)), \tag{11}$$

where ω denotes the observer state vector (the dimension of the vector ω is equal to the dimension of $\tilde{x}$ in the system of Eq. (6)), $\tilde{z}$ is the measured output and L is a matrix chosen so that the eigenvalues of the matrix

$$C_L = \left.\frac{\partial f}{\partial \omega}\right|_{(\omega=\omega_s)} - L \left.\frac{\partial h}{\partial \omega}\right|_{(\omega=\omega_s)},$$

where ω_s is the operating steady-state, lie in the open left-half of the complex plane. The state observer of Eq. (11) consists of a replica of the system of Eq. (6) plus a linear gain multiplying the discrepancy between the actual and the estimated values of the output, and therefore, it is an extended Luenberger-type observer. The combination of the state observer of Eq. (11) with the state feedback controller of Eq. (7) leads to the following nonlinear output feedback controller:

$$\begin{aligned} \frac{d\omega_0}{dt} &= -\omega_0 + (1-\omega_3)Da\, e^{-F/\omega_4^2} + L_0(h(\tilde{x}) - h(\omega)), \\ \frac{d\omega_1}{dt} &= -\omega_1 + \omega_4\omega_0 + L_1(h(\tilde{x}) - h(\omega)), \\ \frac{d\omega_2}{dt} &= -\omega_2 + \omega_4\omega_1 + L_2(h(\tilde{x}) - h(\omega)), \\ \frac{d\omega_3}{dt} &= -\omega_3 + \omega_4\omega_2 + L_3(h(\tilde{x}) - h(\omega)), \\ \frac{d\omega_4}{dt} &= \frac{1-\omega_4-(\alpha-\omega_4)\omega_4\omega_2}{1-\omega_3} + L_4(h(\tilde{x}) - h(\omega)), \\ u &= -k(\omega)L_g V(\omega), \end{aligned} \tag{12}$$

where $L = [L_0\ L_1\ L_2\ L_3\ L_4]^{\mathrm{T}}$ are the observer parameters and $h(\omega) = \omega_0$. The practical implementation of the nonlinear controller of Eq. (12) requires online measurements of the controlled output $\tilde{x}_0$; in practice, such measurements can be obtained by using, for example, light scattering (Bohren and Huffman, 1983; Rawlings et al., 1993) and FBRM (focused-beam reflectance measurement, Barthe and Rousseau, 2006).

2.3. Modeling sensor data loss

Following the approach presented in Mhaskar et al. (2007), sensor data losses are modeled within the framework of random Poisson processes. Specifically, at a given time t an 'event' takes place that determines whether the system will be closed-loop or open-loop (see Fig. 1). For a given rate of data loss $0 \leqslant r \leqslant 1$, a random variable P is chosen from a uniform probability distribution between 0 and 1. If $P \leqslant r$, the event is deemed to be

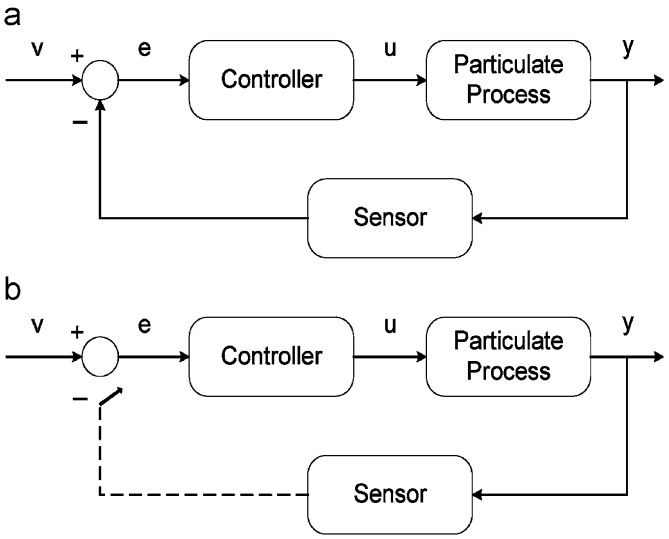

Fig. 1. Closed-loop system in the (a) absence, and (b) presence of sensor data losses.

'measurement loss' (which implies that the process operates in open-loop), while if $P > r$, the event is understood to be 'measurement available' (which implies that the process operates in closed-loop). Furthermore, with W defined as the number of events per unit time, another random variable χ with uniform probability distribution between 0 and 1 determines the time for which the current event will last, given by $\Delta = (-\ln \chi / W)$. At $t + \Delta$ another event takes place and whether it represents a measurement or loss of measurement, as well as its duration, is similarly determined.

Note that in the presence of constraints in the manipulated input, prolonged duration of measurement loss may land the system states at a point starting from where stabilization may not be achievable (even with continuous measurement). Therefore, the presence of manipulated input constraints implies that the sensor data loss rate should be defined over a finite time interval. Specifically, for a positive real number T^*, we define $r \in [0, 1]$ as sensor data loss rates over the finite time interval of duration T^*. This implies that over every successive finite time interval T^*, the measurements are available for a total time of $T^* \times (1 - r)$. Note that this definition does not impose any restrictions on the distribution of sequences of measurement loss and availability over the time interval T^* and does not need to hold for *any* finite interval T^* but only successive time intervals T^* (requiring the data loss rate to hold over *any* fixed finite time interval T^* would be equivalent to require it hold over infinitesimal time intervals). All it says is that over the time interval T^*, if the duration of all the measurement loss events is summed up, then that sum is equal to $T^* \times r$. In simulating data losses, this definition can be practically realized by picking W to be sufficiently large; the reasoning behind this is as follows: a larger value of W increases the number of events per unit time, and when W is sufficiently large, we can get a sufficiently large number of events over every finite time interval T^* such that the rate of data loss is sufficiently close to r.

Table 2
Dimensionless parameter values of the continuous crystallizer

$\sigma = k_1 \tau (c_{0s} - c_s) = 1.0\,\text{mm}$
$Da = 8\pi\sigma^3 k_2 \tau = 200.0$
$F = k_3 c_s^2 / (c_{0s} - c_s)^2 = 3.0$
$\alpha = (\rho - c_s)/(c_{0s} - c_s) = 40.0$

2.4. Simulation results

In this subsection, we apply the state feedback controller of Eq. (7) and output feedback controller of Eq. (12) to the crystallizer process model and evaluate their robustness in the presence of sensor data losses. Specifically, the objective is to compute a data loss rate r^*, defined over a finite time interval T^*, such that if $r < r^*$ then convergence to a desired neighborhood is achieved in the presence of data losses. Note that implicit in this analysis is the understanding that during the time that sensor measurements are unavailable, the values of the measured variables (in computing the control action) are 'frozen' at the last available measurement. This results in the value of the manipulated variable being frozen at the last computed value. Note also, that the value of r^* is expected to depend on the interval T^* over which it is defined (see the simulation example in Mhaskar et al., 2007, for a demonstration). To understand this more clearly, note that for convergence to a desired neighborhood of the origin, one can come up with a value Δ^* such that if only one measurement was received every Δ^*, then convergence to the desired neighborhood would be achieved. The robustness analysis in Mhaskar et al. (2007) exploits this fact together with the definition of the data loss rate, to ensure that over a Δ^* duration within T^* (and across two time intervals), at least one measurement is received. In summary, Δ^* is fixed by the given size of the neighborhood to the origin where convergence is desired (δ'); given a T^* over which the data loss rate is defined, r^* can then in turn be picked such that the maximum duration of open-loop behavior across intervals stays less than Δ^*.

Following the proposed methodology, we first use the reduced moments model of Eq. (5) to design the controllers. The control objective is to suppress the oscillatory behavior of the crystallizer and stabilize it at an unstable steady-state that corresponds to a desired PSD by manipulating the solute feed concentration. The values of the dimensionless model parameters in Eq. (5) can be found in Table 2. The dimensionless solute feed concentration, u, is subject to the constraints: $-u_{\max} \leqslant u \leqslant u_{\max}$. For $u_{\max} = 2$, the constraint on the inlet solute concentration corresponds to $960\,\text{kg/m}^3 \leqslant c_0 \leqslant 1040\,\text{kg/m}^3$ and for $u_{\max} = 4$, the constraint on the inlet solute concentration corresponds to $920\,\text{kg/m}^3 \leqslant c_0 \leqslant 1080\,\text{kg/m}^3$. The desired steady-state is $\tilde{x}^s = [\tilde{x}_0^s\ \tilde{x}_1^s\ \tilde{x}_2^s\ \tilde{x}_3^s\ \tilde{y}^s]' = [0.0652\ 0.0399\ 0.0244\ 0.0149\ 0.6118]'$, and $u^s = 0.2$.

To facilitate the design of the bounded controller and construction of the CLF, we initially rewrite the moments model of Eq. (5) in deviation variable form—thus translating the steady-state to the origin—to obtain the system of Eq. (6) which we transform into the normal form. We introduce the invertible

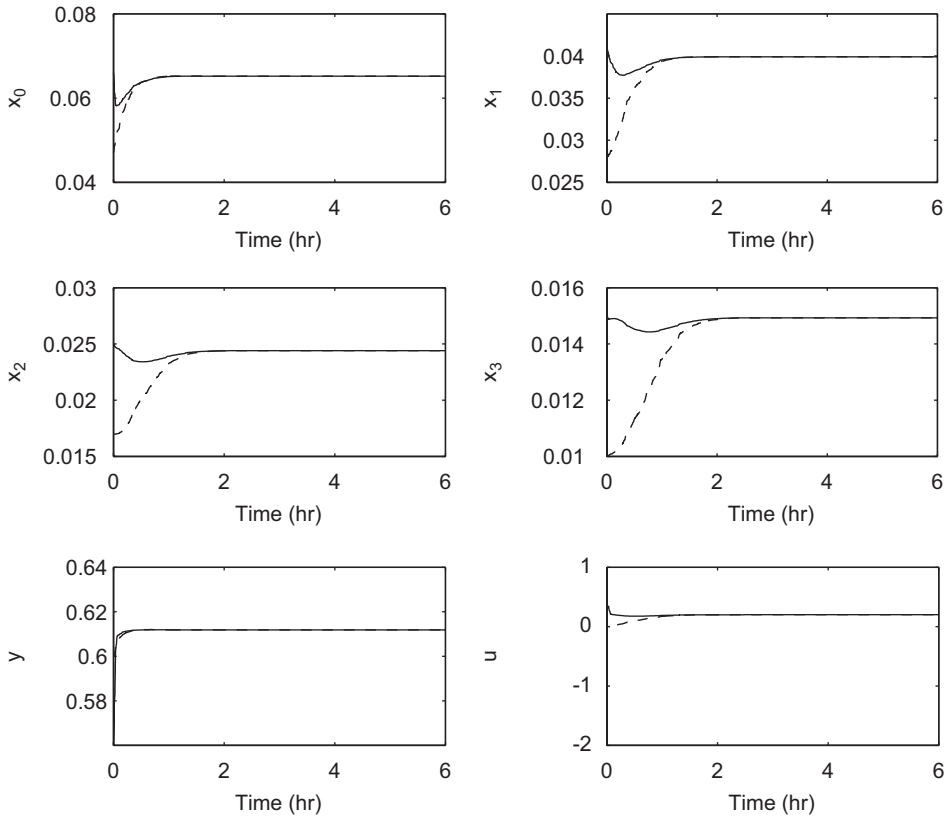

Fig. 2. Evolution of the closed-loop state and input profiles under state feedback control (solid lines) and output feedback control (dashed lines) for $u_{\max} = 2$ and no sensor data losses.

coordinate transformation: $[\xi' \ \eta']' = \Pi(x) = [\tilde{x}_0 \ f_1(\tilde{x}) \ \tilde{x}_1 \ \tilde{x}_2 \ \tilde{x}_3]'$, where $\xi = [\xi_1 \ \xi_2]' = [\tilde{x}_0 \ f_1(\tilde{x})]'$, $\bar{y} = \xi_1$, $f_1(\tilde{x}) = -\tilde{x}_0 + (1 - \tilde{x}_3)Da \exp(-F/\tilde{y}^2)$, and $\eta = [\eta_1 \ \eta_2 \ \eta_3]' = [\tilde{x}_1 \ \tilde{x}_2 \ \tilde{x}_3]'$. The state-space description of the system in the transformed coordinates takes the form

$$\dot{\xi} = A\xi + bl(\xi, \eta) + b\alpha(\xi, \eta)u,$$
$$\dot{\eta} = \Psi(\eta, \xi), \tag{13}$$

where

$$A = \begin{bmatrix} 0 & 1 \\ 0 & 0 \end{bmatrix}, \quad b = \begin{bmatrix} 0 \\ 1 \end{bmatrix}, \quad l(\xi, \eta) = L_f^2 h(\Pi^{-1}(\xi, \eta))$$

is the second-order Lie derivative of the scalar function, $h(\cdot)$, along the vector field $f(\cdot)$, and $\alpha(\xi, \eta) = L_g L_f h(\Pi^{-1}(\xi, \eta))$ is the mixed Lie derivative. The forms of $f(\cdot)$ and $g(\cdot)$ can be obtained by re-writing the system of Eq. (5) in the form of Eq. (6), and are omitted for brevity.

The partially linear ξ-subsystem in Eq. (13) is used to design a bounded controller that stabilizes the full interconnected system of Eq. (13) and, consequently, the original system of Eq. (5). For this purpose, a quadratic function of the form, $V_\xi = \xi' P \xi$, is used as a CLF in the controller synthesis formula of Eqs. (7)–(8), where the positive-definite matrix,

$$P = \begin{bmatrix} 1.7321 & 1.0000 \\ 1.0000 & 1.7321 \end{bmatrix},$$

is chosen to satisfy the Riccati matrix equality: $A'P + PA - Pbb'P = -\bar{Q}$ where

$$\bar{Q} = \begin{bmatrix} 1 & 0 \\ 0 & 1 \end{bmatrix}$$

is a positive-definite matrix. The stability region estimate for the system is obtained as a level set of the Lyapunov function. For details on how to construct estimate of the stability regions for this system, see Shi et al. (2006). We initialize the crystallizer model at the following initial conditions $[\tilde{x}_0(0) \ \tilde{x}_1(0) \ \tilde{x}_2(0) \ \tilde{x}_3(0) \ \tilde{y}(0)]' = [0.066 \ 0.041 \ 0.025 \ 0.015 \ 0.560]'$ and initialize the observer at $[\omega_0(0) \ \omega_1(0) \ \omega_2(0) \ \omega_3(0) \ \omega_4(0)]' = [0.047 \ 0.028 \ 0.017 \ 0.010 \ 0.5996]'$. The matrix L was chosen as $L = [L_0 \ L_1 \ L_2 \ L_3 \ L_4]' = [1 \ 0 \ 0 \ 0 \ 0]'$ to satisfy the requirement that the eigenvalues of the matrix

$$C_L = \left.\frac{\partial f}{\partial \omega}\right|_{(\omega=\omega_s)} - L \left.\frac{\partial h}{\partial \omega}\right|_{(\omega=\omega_s)},$$

where ω_s is the operating steady-state, lie in the open left-half of the complex plane.

We pick the value of number of events to be $W = 400$ events per hour. Fig. 2 shows the evolution of the closed-loop state (and state estimates in the case of output feedback control) and input profiles with $u_{\max} = 2$ and no sensor losses under both state feedback control (solid lines) and output feedback control

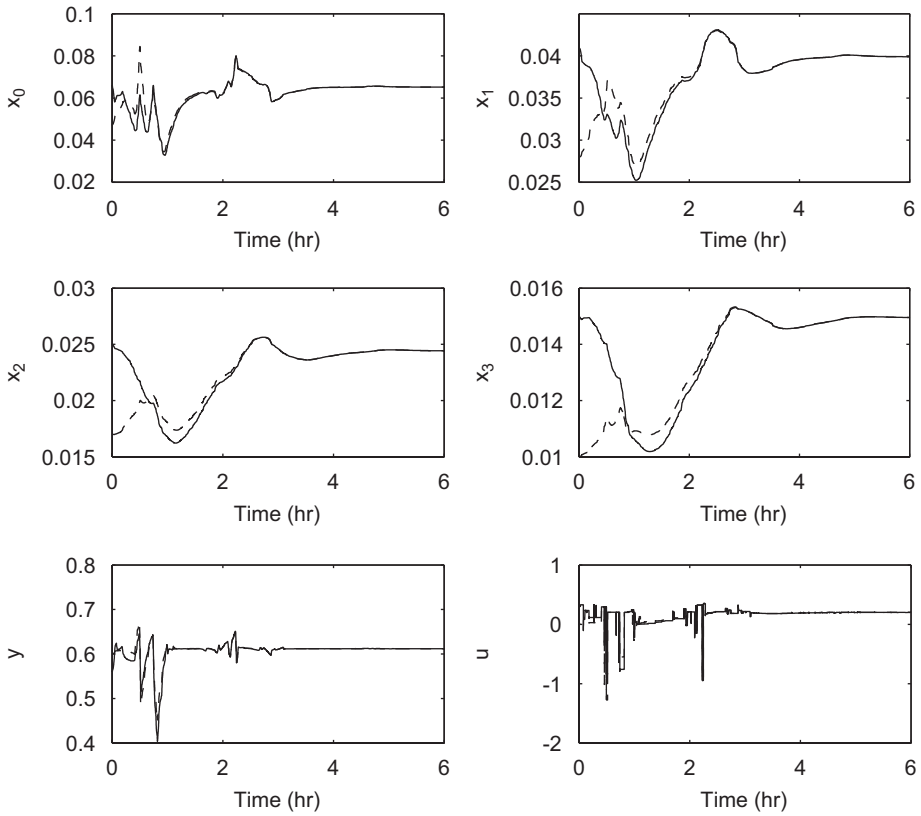

Fig. 3. Evolution of the closed-loop state (and state estimates in the case of output feedback control) and input profiles under state feedback control (solid lines) and output feedback control (dashed lines) for $u_{max} = 2$ and 90% probability of sensor data losses.

(dashed lines). In both cases, we observe that the states of the closed-loop system converge to the desired steady-state. Fig. 3 shows the evolution of the closed-loop state (and state estimates in the case of output feedback control) and input profiles with $u_{max} = 2$ and 90% probability of sensor losses. Even though the amount of losses is very significant, both the state feedback controller (solid lines) and the output feedback controller (dashed lines) achieve stabilization of the process at the desired steady-state. However, if the sensor data loss rate is 95% closed-loop stability under both state feedback (solid lines) and output feedback control cannot be achieved (dashed lines), see Fig. 4. We did not observe a significant difference between state feedback control and output feedback control in the sensor data loss rate for which closed-loop stability is preserved. This is expected due to the nature of the system dynamics. Specifically, we observed that even with continued open-loop operation, the process stays in a region such that if continuous measurements are received from a certain point in time onwards, closed-loop stability is achieved. The output feedback problem, up until the time that the state has not converged to the true values can be thought of as open-loop operation, however, once the state estimates converge then the problem 'reverts' to the state feedback problem and the preservation of closed-loop stability depends only on the data loss rate.

We also investigated the effect of different magnitude of manipulated input constraints on the sensor data loss rate that ensures closed-loop stability. Fig. 5 shows the evolution of the state and input profiles with $u_{max} = 4$ and no sensor data losses. The states of the closed-loop system under both state feedback control (solid lines) and output feedback control (dashed lines) converge to the steady-state. Fig. 6 shows the evolution of the state and input profiles with $u_{max} = 4$ and 70% probability of sensor data losses. In this case, closed-loop stability is maintained. However, when the data loss rate increases to 75% closed-loop stability is not achieved under both state feedback control (solid lines) and output feedback control (dashed lines), see Fig. 7.

The reduced data loss rate under larger input constraints is expected because larger input constraints means that the input has a stronger effect on the process which implies that large time intervals of open-loop behavior of the manipulated input (when data losses occur) have an increased destabilizing effect on the closed-loop system. Table 3 summarizes r^* values for different u_{max}; the larger the manipulated input constraint, the more sensitive the system toward sensor data loss. This observation also suggests that if excessive data loss rate occurs, the value of u_{max} can be artificially reduced to accommodate the data loss and if the current state resides in the stability region with the reduced u_{max}, closed-loop stability can be preserved.

3. Handling sensor malfunctions: batch crystallizer

In this section, we consider a batch particulate process and address the problem of producing PSD at the end of the batch

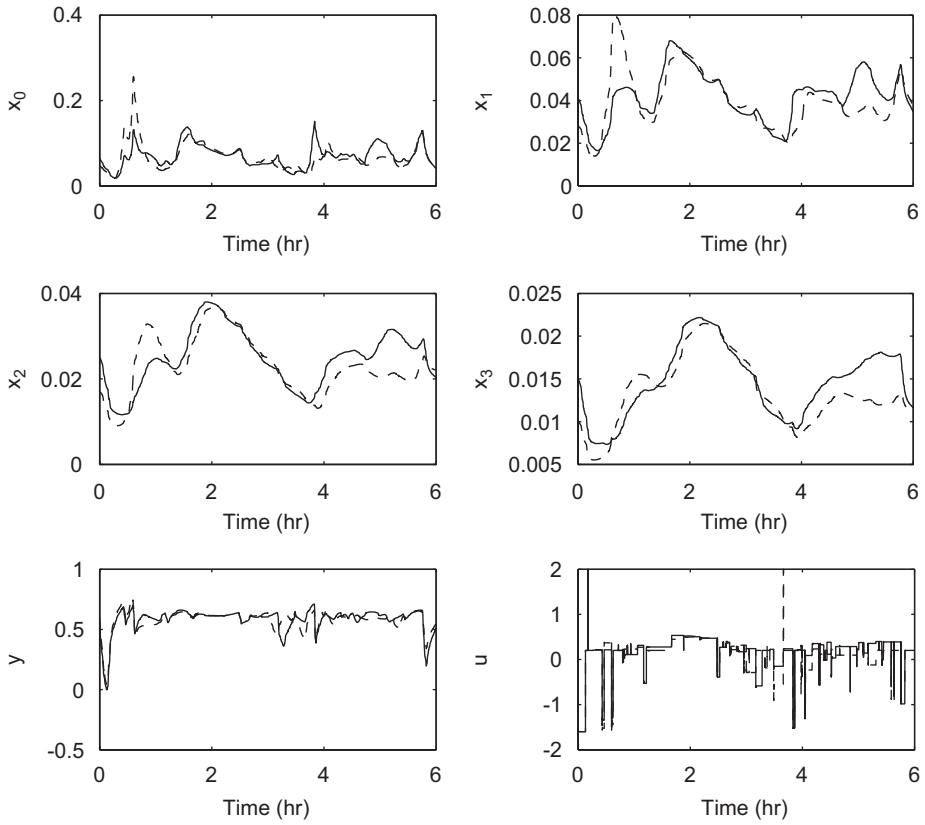

Fig. 4. Evolution of the closed-loop state (and state estimates in the case of output feedback control) and input profiles under state feedback control (solid lines) and output feedback control (dashed lines) for $u_{\max} = 2$ and 95% probability of sensor data losses.

that has desired characteristics while satisfying state and control constraints during the batch and handling sensor data losses.

3.1. PBM of a protein batch crystallizer

The batch crystallizer considered in this work is taken from our previous work (see Shi et al., 2005). A PBM is used to describe the evolution of the crystal size distribution (CSD), $n(r,t)$. The evolution of the solute concentration, C, and crystallizer temperature, T, are described by two ODEs. The process model has the following form:

$$\frac{\partial n(r,t)}{\partial t} + G(t)\frac{\partial n(r,t)}{\partial r} = 0, \quad n(0,t) = \frac{B(t)}{G(t)},$$

$$\frac{\mathrm{d}C}{\mathrm{d}t} = -24\rho k_v G(t)\mu_2(t),$$

$$\frac{\mathrm{d}T}{\mathrm{d}t} = -\frac{UA}{MC_p}(T - T_j), \tag{14}$$

where $G(t)$ is the growth rate, $B(t)$ is the nucleation rate, ρ is the density of crystals, k_v is the volumetric shape factor, U is the overall heat-transfer coefficient, A is the total heat-transfer surface area, M is the mass of solvent in the crystallizer, C_p is the heat capacity of the solution, T_j is the jacket temperature and $\mu_2 = \int_0^\infty r^2 n(r,t)\,\mathrm{d}r$ is the second moment of the CSD. The crystal nucleation rate $B(t)$ (Galkin and Vekilov, 1999; Bhamidi et al., 2002) is given by an equation of the following form:

$$B(t) = k_a C \exp\left(-\frac{k_b}{\sigma^2}\right), \tag{15}$$

where k_a and k_b are parameters that are obtained using experimental results. The supersaturation, σ, is the concentration of the solution in excess of the saturation concentration (solubility) and is understood to be the driving force for the crystal nucleation and growth. The supersaturation is defined as

$$\sigma = \ln(C/C_s), \tag{16}$$

where C is the solute concentration and C_s is the solubility and expressed as follows:

$$C_s(T) = 1.0036 \times 10^{-3}T^3 + 1.4059 \times 10^{-2}T^2 - 0.12835T + 3.4613 \tag{17}$$

as a result of third-order polynomial data fitting based on solubility data in Sazaki et al. (1996). Eq. (17) exhibits trends similar to the experimental solubility data of being low at low temperature and increasing significantly with increasing temperature. The crystal growth rate $G(t)$ is derived based on an empirical model to describe the growth rate of the tetragonal

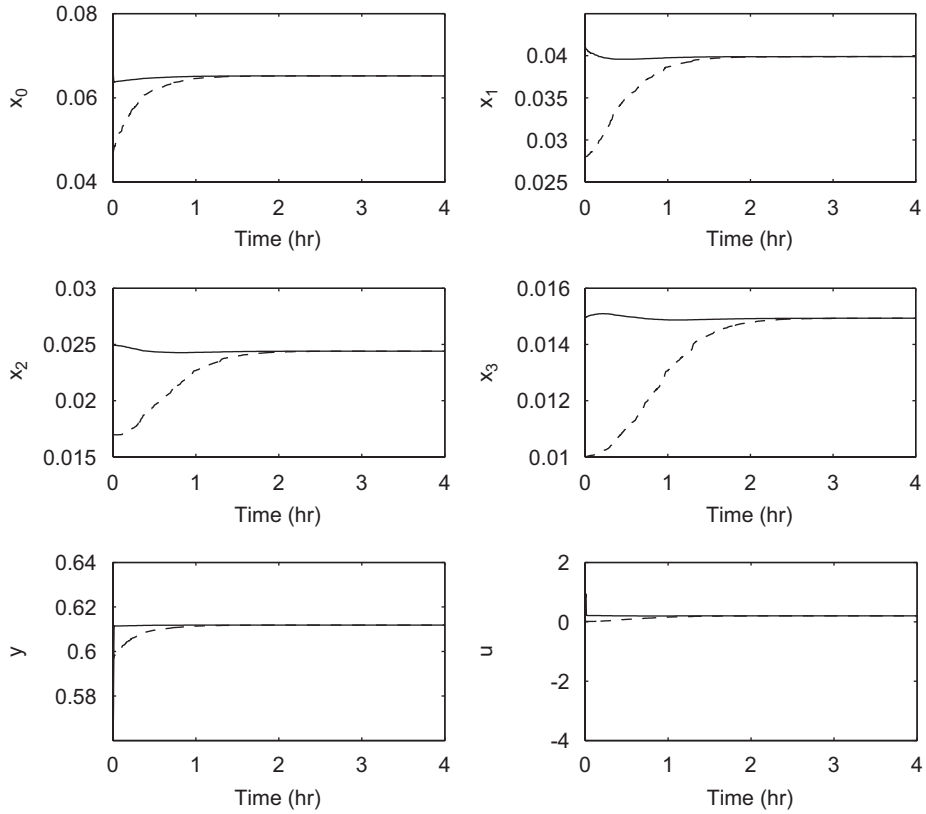

Fig. 5. Evolution of the closed-loop state (and state estimates in the case of output feedback control) and input profiles under state feedback control (solid lines) and output feedback control (dashed lines) for $u_{\max} = 4$ and no sensor data losses.

HEW lysozyme crystals as a function of supersaturation in the following form:

$$G(t) = k_g \sigma^g, \tag{18}$$

where k_g is the pre-exponential factor of the growth rate. Parameter values for this model are given in Table 4. Note that because of the tetragonal form of the crystals and the existence of about 46% of solvent in each crystal (Leung et al., 1999), the volumetric shape factor, k_v, is set equal to 0.54.

The fact that the dominant dynamics of the crystallizer are characterized by a small number of degrees of freedom (Chiu and Christofides, 1999), method of moments (Hulburt and Katz, 1964) (see also Christofides, 2002; Shi et al., 2006; Mantzaris and Daoutidis, 2004) is applied to the system of Eq. (14) to derive an approximate ODE model. Defining the ith moment of $n(r, t)$ as

$$\mu_i = \int_0^\infty r^i n(r, t)\, \mathrm{d}r, \quad i = 0, 1, \ldots, \infty \tag{19}$$

multiplying the population balance in Eq. (14) by r^i, and integrating over all crystal sizes, the following infinite set of ODEs, which describes the rate of change of the moments of the crystal size distribution, solute concentration and temperature, is obtained

$$\begin{aligned}
\frac{\mathrm{d}\mu_0}{\mathrm{d}t} &= B(t),\\
\frac{\mathrm{d}\mu_i}{\mathrm{d}t} &= \mathrm{i}G(t)\mu_{i-1}(t), \quad i = 1, 2, \ldots, \infty,\\
\frac{\mathrm{d}C}{\mathrm{d}t} &= -24\rho k_v G(t)\mu_2(t),\\
\frac{\mathrm{d}T}{\mathrm{d}t} &= -\frac{UA}{MC_p}(T - T_j).
\end{aligned} \tag{20}$$

Note that in Eq. (20), the ODEs describing the dynamics of the first N moments, where N is any positive integer greater than or equal to 3, the solute concentration and the crystallizer temperature are independent of the moments of order $N + 1$ and higher. This implies that a set of ordinary differential equations, which include the first N moments and the evolution of the solute concentration and crystallizer temperature, would provide an accurate description of the evolution of the first N moments, the solute concentration and the crystallizer temperature.

As will be seen in Section 3.3, the control objective will require computation of μ_3 and μ_4, hence N is chosen as 4 and the following reduced-order model is used for the purpose of

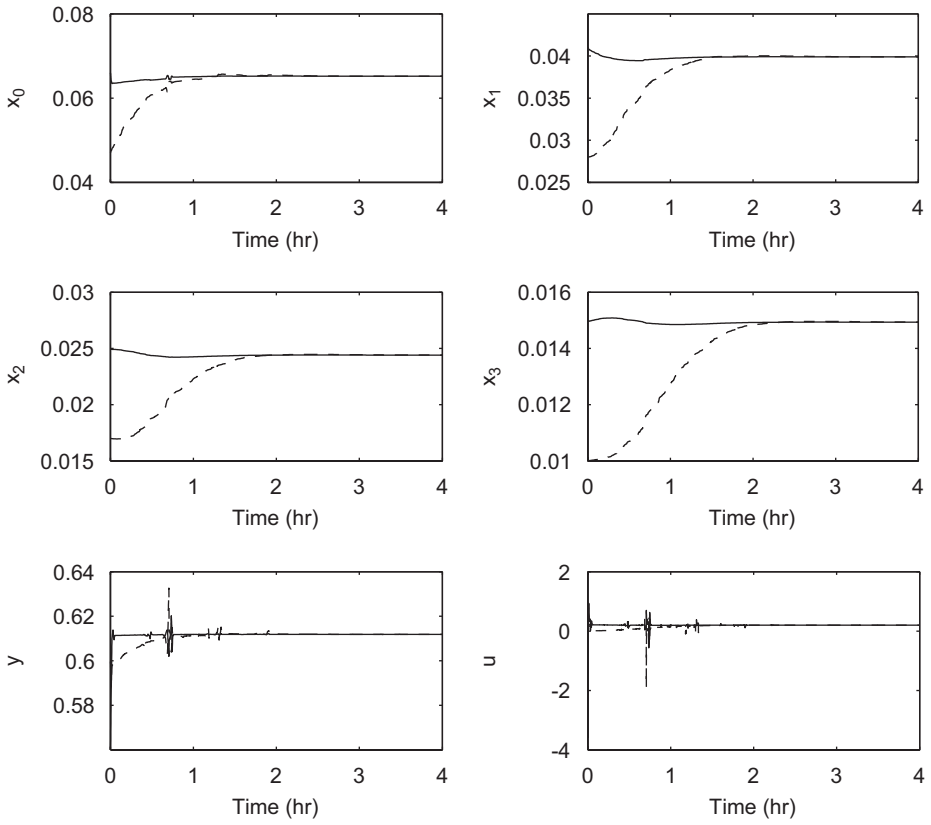

Fig. 6. Evolution of the closed-loop state (and state estimates in the case of output feedback control) and input profiles under state feedback control (solid lines) and output feedback control (dashed lines) for $u_{\max} = 4$ and 70% probability of sensor data losses.

controller design:

$$\begin{aligned}
\frac{d\mu_0}{dt} &= B(t),\\
\frac{d\mu_i}{dt} &= iG(t)\mu_{i-1}(t), \quad i = 1, 2, 3, 4,\\
\frac{dC}{dt} &= -24\rho k_v G(t)\mu_2(t),\\
\frac{dT}{dt} &= -\frac{UA}{MC_p}(T - T_j).
\end{aligned} \tag{21}$$

3.2. State estimator design

In this section, we present an observer design that uses measurements of the solute concentration, C, and temperature T and the reduced order moments model, to generate estimates of the moments. Similar to the continuous crystallizer example, an extended Luenberger-type observer is used to estimate the values of the moments of the CSD and takes the following form:

$$\begin{aligned}
\frac{d\hat{\mu}_0}{dt} &= \hat{B}(t) + L_0(C_m - \hat{C}),\\
\frac{d\hat{\mu}_i}{dt} &= i\hat{G}(t)\hat{\mu}_{i-1}(t) + L_i(C_m - \hat{C}), \quad i = 1, \ldots, 4,\\
\frac{d\hat{C}}{dt} &= -24\rho k_v \hat{G}(t)\hat{\mu}_2(t) + L_5(C_m - \hat{C}),
\end{aligned} \tag{22}$$

where C_m is the online measurement of the solute concentration, $\hat{B}(t)$ and $\hat{G}(t)$ are the nucleation and growth rates computed using the online measurement of T and values of the estimates of $\hat{\mu}_i$ and $\hat{C}$, and L_i, $i = 0, \ldots, 5$ are the observer gains (these values were obtained via running open-loop simulations and comparing the evolution of the state with the state estimates for different choices of the observer gains), reported in Table 5.

Note that since the states μ_3 and μ_4 do not effect the evolution of the concentration, these states are not observable from the concentration measurements. For the batch crystallization considered in this work, the initial values of the moments at the beginning of the batch run are identically equal to 0, because there are no crystals initially inside the crystallizer. In the case of a perfect model, therefore, the state estimates are naturally initialized at the true values and would continue to track the true values. In the case of plant-model mismatch, the observer continues to generates satisfactory estimates of the observable states.

3.3. Predictive controller formulation and closed-loop results

In the case of continuous crystallizer operation, the overriding objective is often stabilization, and the presence of constraints on the manipulated input limits the set of initial conditions starting from where stabilization can be achieved. For batch processes, in contrast, the expression of performance

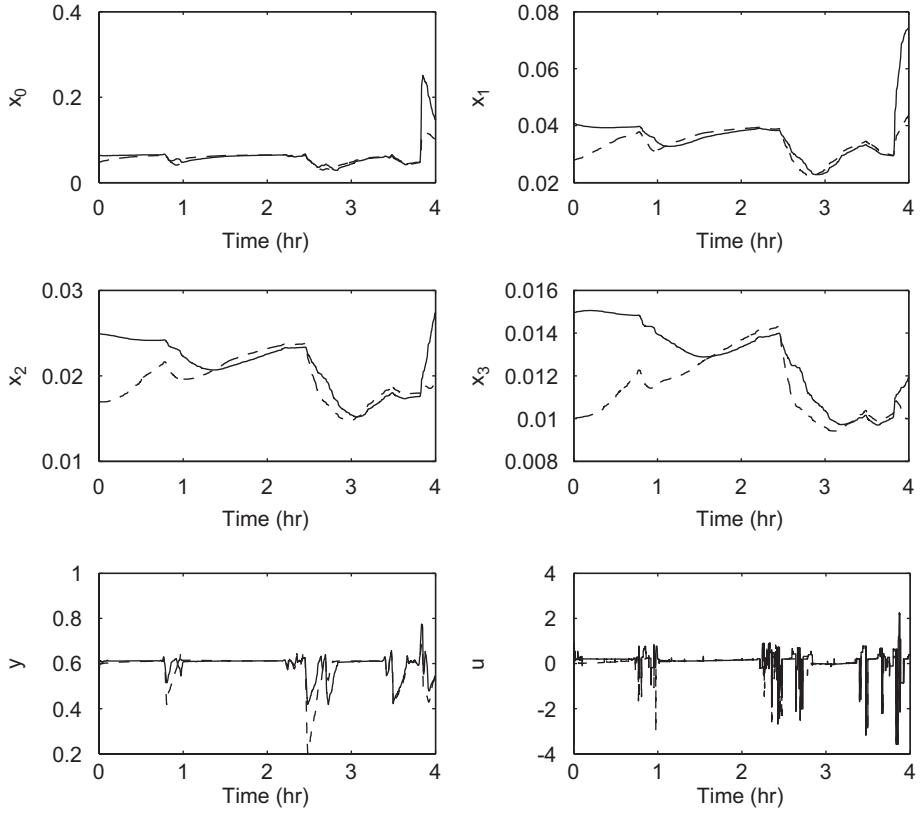

Fig. 7. Evolution of the closed-loop state (and state estimates in the case of output feedback control) and input profiles under state feedback control (solid lines) and output feedback control (dashed lines) for $u_{\max} = 4$ and 75% probability of sensor data losses.

Table 3
Summary of r^* values for different $u_{\max}$ for the continuous crystallizer example

$u_{\max}$	r^* (% sensor data loss)
1	0.05 (95)
2	0.10 (90)
3	0.20 (80)
4	0.30 (70)
6	0.35 (65)

Table 4
Parameter values for the batch crystallizer model of Eqs. (14)–(18)

k_a	1044.4/(min cm^3)	k_g	3.1451×10^{-9} cm/ min
k_b	51.33	g	5.169
k_v	0.54	ρ	1.40×10^3 mg/cm^3
U	1800 kJ/m^2 h K	A	0.25 m^2
M	10 kg	C_p	4.13 kJ/K kg

considerations in the form of appropriate constraints or through the objective function, and the achievement of a PSD that has the desired characteristics, is an important issue. Based on these considerations, we present in the remainder of this section a predictive controller formulation where, at time t_i, the control trajectory is computed by solving an optimization problem of the form:

$$
\begin{aligned}
\min \quad & -\frac{\mu_4(t_f)}{\mu_3(t_f)} \\
\text{s.t.} \quad & \frac{\mathrm{d}\mu_0}{\mathrm{d}t} = k_a C \exp\left(-\frac{k_b}{\sigma^2}\right), \\
& \frac{\mathrm{d}\mu_i}{\mathrm{d}t} = \mathrm{i}k_g \sigma^g \mu_{i-1}(t), \quad i = 1, \ldots, 4, \\
& \frac{\mathrm{d}C}{\mathrm{d}t} = -24\rho k_v k_g \sigma^g \mu_2(t), \\
& \frac{\mathrm{d}T}{\mathrm{d}t} = -\frac{UA}{MC_p}(T - T_j), \\
& \mu_i(t_i) = \hat{\mu}_i(t_i), \\
& C(t_i) = \hat{C}(t_i), \\
& t_i \leqslant t \leqslant t_f, \\
& T_{\min} \leqslant T \leqslant T_{\max}, \\
& T_{j\,\min} \leqslant T_j \leqslant T_{j\,\max}, \\
& \sigma_{\min} + \varepsilon \leqslant \sigma \leqslant \sigma_{\max} - \varepsilon, \\
& \left|\frac{\mathrm{d}C_s}{\mathrm{d}t}\right| \leqslant k_1,
\end{aligned}
\tag{23}
$$

Table 5
Parameter values for the Luenberger-type observer of Eq. (22)

L_0	−0.4	L_1	0.05
L_2	0.001	L_3	1.7×10^{-5}
L_4	3×10^{-7}	L_5	−0.1

$$\frac{B(t)}{G(t)} \leqslant n_{\text{fine}}, \quad \forall t \geqslant t_f/2, \tag{24}$$

where μ_4/μ_3 is the volume-averaged crystal size, $T_{\min}$ and $T_{\max}$ are the constraints on the crystallizer temperature, T, and are specified as 4 and 22 °C, respectively. $T_{j\,\min}$ and $T_{j\,\max}$ are the constraints on the manipulated variable, T_j, and are specified as 3 and 22 °C, respectively. The constraints on the supersaturation σ are $\sigma_{\min} = 1.72$ and $\sigma_{\max} = 2.89$. The constant, k_1 (chosen to be 0.065 mg/ml min), specifies the maximum rate of change of the saturation concentration C_s. n_{fine} is the largest allowable number of nuclei at any time instant during the second half of the batch run, and is set to 5/μm ml. The parameter ε is used to allow for tightening of the constraints in the controller to enable constraint satisfaction for the system in the presence of sensor data losses and plant model mismatch. In the context of batch crystallizer control, previous work has shown that the objective of maximizing the volume-averaged crystal size can result in a large number of fines in the final product (Ma et al., 2002). Therefore, the constraint of Eq. (24) restricts the number of nuclei formed at any time instant during the second half of the batch run in order to limit the fines in the final product. Measurements of the solute concentration and the crystallizer temperature are assumed to be available; Δ_m, the maximum possible delay between two successive measurements, is taken as 5 min. The measurements are used by the Luenberger-type observer to generate estimates of the moments, which are used as initial conditions of the states in the moments model. t_f, the total batch time, is chosen as 24 h. The optimization problem is solved using sequential quadratic programming (SQP). A second-order accurate finite difference scheme with 3000 discretization points is used to obtain the solution of the PBM of Eq. (14).

We apply the control action computed by the low-order predictive controller of Eq. (23) on the PBM and study the problem of constraint satisfaction in the presence of sensor data losses and model uncertainty. Specifically, we consider a case of process-model mismatch by changing the value of the parameter g (the exponent relating growth rate to supersaturation) from its nominal value of 5.169 to 4.652 (a 10% change) in the predictive controller. We first show simulation results with maximum duration between successive measurement of $\Delta_m = 5$ min and ε in Eq. (23) is 0. Solid lines in Fig. 8 depict the implementation of the predictive controller where the state constraints are satisfied for the entire batch run and the performance objective is achieved (the supersaturation is within the lower and upper bounds, $1.72 \leqslant \sigma \leqslant 2.89$). Note that the possible errors in the values of the unobservable states has an impact on the achievement of the product properties as described by the objective function. However, the satisfactory estimation

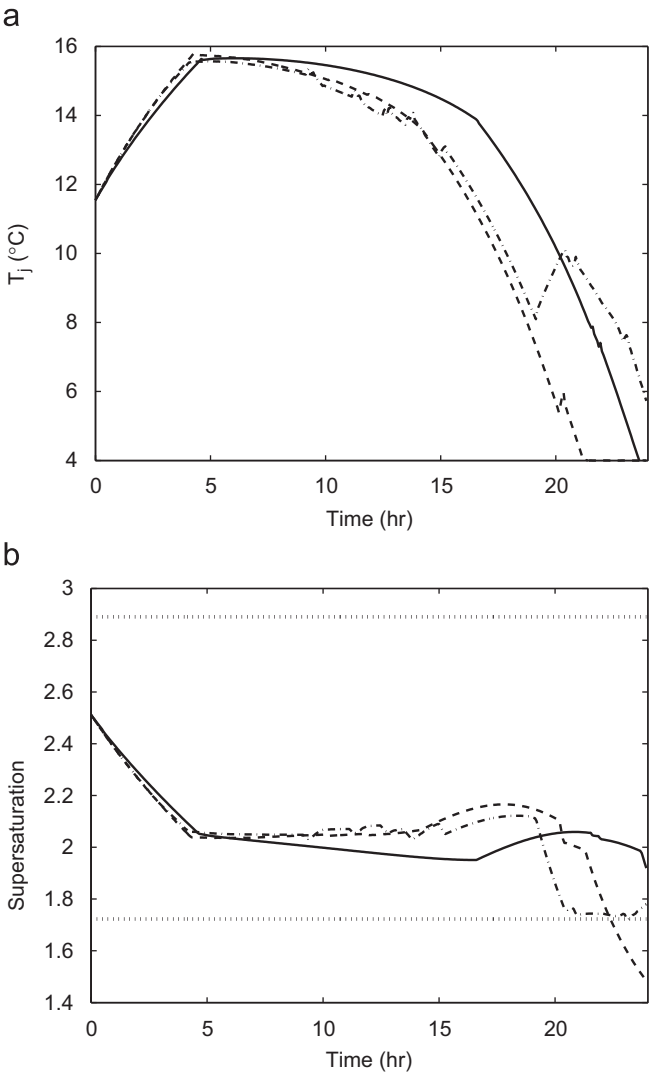

Fig. 8. (a) Jacket temperature and (b) supersaturation profiles under output feedback control; sampling time of 5 min (solid lines), sampling time of 10 min without constraint modification (dashed lines) and sampling time of 10 min under the predictive controller with tightened constraints (dash-dotted lines).

of the observable states and the expression of the performance considerations as constraints on the observable states allows the achievement of most of the desired properties at the end of the batch run. Consider now the case where, due to sensor data losses, the maximum duration between successive measurement increases from $\Delta_m = 5$ to 10 min. Implementation of the predictive controller of Eq. (23), with the same values of controller parameters as before ($1.72 \leqslant \sigma \leqslant 2.89$), leads to violation of the state constraints (see dashed lines in Fig. 8). To alleviate the problem of state constraint violation in the presence of sensor data losses, we implement the controller of Eq. (23) with a tightened constraint on the supersaturation $\varepsilon = 0.24$ ($1.96 \leqslant \sigma \leqslant 2.65$). As can be seen by the dotted lines in Fig. 8, the predictive controller is able to successfully achieve the performance objective (the supersaturation is within the lower and upper bound, $1.72 \leqslant \sigma \leqslant 2.89$), while at the same

time respecting the state and input constraints in the presence of sensor data losses.

4. Conclusions

This work investigated the problem of preserving closed-loop stability and performance of feedback control of particulate processes in the presence of sensor data losses. To demonstrate the issue of sensor data losses in the context of specific process applications, two typical particulate process examples, a continuous crystallizer and a batch protein crystallizer, were considered and modeled by PBMs. In both examples, feedback control systems was first designed on the basis of low-order models and applied to the PBMs to enforce closed-loop stability and constraint satisfaction. Subsequently, the robustness of the control systems in the presence of sensor data losses was investigated. Specifically, in the case of the continuous crystallizer, a Lyapunov-based nonlinear output feedback controller was designed and was shown to stabilize an open-loop unstable steady-state of the PBM in the presence of input constraints. It was demonstrated that this controller is robust with respect to significant sensor data losses but, as expected, it cannot maintain closed-loop stability when the sensor data losses exceed a certain threshold. In the case of the batch crystallizer, a predictive controller was first designed to obtain a desired crystal size distribution at the end of the batch while satisfying state and input constraints. In the presence of sensor data losses, we pointed out how the constraints in the predictive controller can be modified as a means of achieving constraint satisfaction in the closed-loop system in the presence of data losses.

Acknowledgment

Financial support from NSF, CTS-0529295, is gratefully acknowledged.

References

Barthe, S., Rousseau, R.W., 2006. Utilization of focused beam reflectance measurement in the control of crystal size distribution in a batch cooled crystallizer. Chemical Engineering & Technology 29, 206–211.

Bhamidi, V., Varanasi, S., Schall, C.A., 2002. Measurement and modeling of protein crystal nucleation kinetics. Crystal Growth & Design 2, 395–400.

Bohren, C.F., Huffman, D.R., 1983. Absorption and Scattering of Light by Small Particles. Wiley, New York.

Braatz, R.D., Hasebe, S., 2002. Particle size and shape control in crystallization processes. In: Rawlings, J.B. et al. (Eds.), A.I.Ch.E. Symposium Series: Proceedings of the Sixth International Conference on Chemical Process Control, pp. 307–327.

Chiu, T., Christofides, P.D., 1999. Nonlinear control of particulate processes. A.I.Ch.E. Journal 45, 1279–1297.

Chiu, T., Christofides, P.D., 2000. Robust control of particulate processes using uncertain population balances. A.I.Ch.E. Journal 46, 266–280.

Christofides, P.D., 2002. Model-Based Control of Particulate Processes. Kluwer Academic Publishers, Dordrecht.

Christofides, P.D., El-Farra, N.H., Li, M.H., Mhaskar, P., 2007. Model-based control of particulate processes. Chemical Engineering Science, in press.

Daoutidis, P., Henson, M., 2002. Dynamics and control of cell populations. In: Rawlings, J.B. et al. (Eds.), A.I.Ch.E. Symposium Series: Proceedings of the Sixth International Conference on Chemical Process Control, pp. 274–289.

Doyle, F.J., Soroush, M., Cordeiro, C., 2002. Control of product quality in polymerization processes. In: Rawlings, J.B. et al. (Eds.), A.I.Ch.E. Symposium Series: Proceedings of the Sixth International Conference on Chemical Process Control, pp. 290–306.

El-Farra, N.H., Christofides, P.D., 2001. Integrating robustness, optimality and constraints in control of nonlinear processes. Chemical Engineering Science 56, 1841–1868.

El-Farra, N.H., Christofides, P.D., 2003. Bounded robust control of constrained multivariabe nonlinear processes. Chemical Engineering Science 58, 3025–3047.

El-Farra, N.H., Chiu, T., Christofides, P.D., 2001. Analysis and control of particulate processes with input constraints. A.I.Ch.E. Journal 47, 1849–1865.

El-Farra, N.H., Gani, A., Christofides, P.D., 2005. Fault-tolerant control of process systems using communication network. A.I.Ch.E. Journal 51, 1665–1682.

Galkin, O., Vekilov, P.G., 1999. Direct determination of the nucleation rates of protein crystals. Journal of Physical Chemistry B 103, 10965–10971.

Hulburt, H.M., Katz, S., 1964. Some problems in particle technology: a statistical mechanical formulation. Chemical Engineering Science 19, 555–574.

Jerauld, G.R., Vasatis, Y., Doherty, M.F., 1983. Simple conditions for the appearance of sustained oscillations in continuous crystallizers. Chemical Engineering Science 38, 1675–1681.

Kalani, A., Christofides, P.D., 1999. Nonlinear control of spatially-inhomogeneous aerosol processes. Chemical Engineering Science 54, 2669–2678.

Lei, S.J., Shinnar, R., Katz, S., 1971. The stability and dynamic behavior of a continuous crystallizer with a fines trap. A.I.Ch.E. Journal 17, 1459–1470.

Leung, A.K.W., Park, M.M.V., Borhani, D.W., 1999. An improved method for protein crystal density measurements. Journal of Applied Crystallography 32, 1006–1009.

Lin, Y., Sontag, E.D., 1991. A universal formula for stabilization with bounded controls. Systems & Control Letters 16, 393–397.

Ma, D.L., Tafti, D.K., Braatz, R.D., 2002. Optimal control and simulation of multidimensional crystallization processes. Computers & Chemical Engineering 26, 1103–1116.

Mantzaris, N.V., Daoutidis, P., 2004. Cell population balance modeling and control in continuous bioreactors. Journal of Process Control 14, 775–784.

Mhaskar, P., Gani, A., El-Farra, N.H., McFall, C., Christofides, P.D., Davis, J.F., 2006. Integrated fault-detection and fault-tolerant control of process systems. A.I.Ch.E. Journal 52, 2129–2148.

Mhaskar, P., Gani, A., McFall, C., Christofides, P.D., Davis, J.F., 2007. Fault-tolerant control of nonlinear process systems subject to sensor faults. A.I.Ch.E. Journal 53, 654–668.

Ramkrishna, D., 1985. The status of population balances. Reviews in Chemical Engineering 3, 49–95.

Rawlings, J.B., Miller, S.M., Witkowski, W.R., 1993. Model identification and control of solution crystallization processes—a review. Industrial & Engineering Chemistry Research 32, 1275–1296.

Sazaki, G., Kurihara, K., Nakada, T., Miyashita, S., Komatsu, H., 1996. A novel approach to the solubility measurement of protein crystals by two-beam interferometry. Journal of Crystal Growth 169, 355–360.

Shi, D., Mhaskar, P., El-Farra, N.H., Christofides, P.D., 2005. Predictive control of crystal size distribution in protein crystallization. Nanotechnology 16, S562–S574.

Shi, D., El-Farra, N.H., Li, M., Mhaskar, P., Christofides, P.D., 2006. Predictive control of particle size distribution in particulate processes. Chemical Engineering Science 61, 268–281.

Xie, W., Rohani, S., Phoenix, A., 2001. Dynamic modeling and operation of a seeded batch cooling crystallizer. Chemical Engineering Communications 187, 229–249.

Zhang, G.P., Rohani, S., 2003. On-line optimal control of a seeded batch cooling crystallizer. Chemical Engineering Science 58, 1887–1896.